Damage mechanisms of adhesively bonded joints of thin tow-based discontinuous composites

Composites Part C: Open Access 19 (2026) 100690

Contents lists available at ScienceDirect

Composites Part C: Open Access

journal homepage: www.sciencedirect.com/journal/composites-part-c-open-access

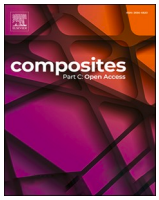

Damage mechanisms of adhesively bonded joints of thin tow-based discontinuous composites

Ioannis Katsivalis [a,b,1,*], Rosemere de Araujo Alves Lima [c,d,1], Florence Moreau [e], Leif E. Asp [b], Sofia Teixeira de Freitas [c,d]

[a] Department of Architecture & Civil Engineering, University of Bath, UK
[b] Department of Industrial and Materials Science, Chalmers University of Technology, Sweden
[c] Faculty of Aerospace Engineering, Delft University of Technology, the Netherlands
[d] IDMEC, Instituto Superior Técnico, Portugal
[e] Oxeon AB, Sweden

ARTICLE INFO

Keywords:
Discontinuous fibre composites
Adhesive bonding
Acoustic Emission (AE)
Scanning Electron Microscopy (SEM)

ABSTRACT

Tow-Based Discontinuous Composites (TBDCs) are a new class of composite materials that combine high strength and stiffness with in-plane isotropy making them of interest in high-end structural applications. Despite their potential, efficient connection methods are currently lacking and the adhesive bonding behaviour of TBDC structures remains unexplored. This work, therefore, seeks to address this gap by analysing the quasi-static performance of TBDC adhesive joints under mode I loading condition. Double Cantilever Beam (DCB) tests were performed using two adhesives with contrasting toughness levels: a moderate (~600 J/m ^{2}) and a high toughness adhesive (> 2400 J/m^2). When a moderate-toughness adhesive was used, a combination of cohesive failure and composite damage was observed, with only a small scatter in the experimental results. In contrast, the use of the high-toughness adhesive led to a shift in damage mechanisms towards the composite micro-architecture, resulting in fracture toughness values in the region of 800 J/m^2, with a larger experimental scatter. Acoustic Emission analysis identified matrix cracking and fibre/matrix debonding as the dominant damage mechanisms. These findings were validated by the post-mortem fractography analysis via Scanning Electron Microscopy. This work therefore provides the first detailed analysis of the damage mechanism in adhesively bonded TBDCs, which have potential in aerospace and automotive applications.

1. Introduction

Carbon Fibre Reinforced Polymer (CFRP) materials are being used extensively in the design of aerospace structures since they combine high strength and stiffness in the fibre direction with low density compared to their metal counterparts. However, composites also display reduced strength and stiffness properties in the transverse and the out-of-plane directions governed by the matrix's (and not the fibre's) properties. Quasi-isotropic layups are typically employed to introduce in-plane isotropic properties, which can simplify the design, but also reduce the structural efficiency of the composite material.

Tow-Based Discontinuous Composites (TBDCs) are based on a random tape orientation distribution that leads to in-plane isotropy while ensuring high fibre volume fractions [1–4]. Using thin tapes to manufacture the TBDCs increases the strength significantly and shifts the damage mechanism from longitudinal and transverse tape fracture to tape pull-out at higher strain levels, increasing the mechanical properties under tension, compression and fatigue loading [5–7]. This is related to the "in-situ strength" effect [8], which delays matrix micro-cracking and delamination and promotes fibre damage in the composite [9]. In addition, large experimental scatter has been reported in the mechanical properties of TBDCs due to the random micro-architecture by multiple authors [5,10,11]. Therefore, assembling such TBDC components, can be a significant engineering challenge.

Adhesive bonding is an efficient method for joining components of a full-scale structure. Adhesive joints do not require drilling, which introduces local defects and stress concentrations and distributes the stresses over the area of the joint [12]. In addition, adhesive joints are a

* Corresponding author.
E-mail address: ik376@bath.ac.uk (I. Katsivalis).
[1] Ioannis Katsivalis and Rosemere de Araujo Alves Lima have contributed equally to the manuscript and are joint first authors.

https://doi.org/10.1016/j.jcomc.2025.100690

Available online 2 January 2026

lightweight solution compared to riveted and bolted joints, which is a key parameter in the structural design of aerospace structures. However, adhesive joints also generate significant peel stresses, hindering the structure's performance and the composite's out-of-plane properties [13,14]. In addition, assessing the performance of adhesive joints and monitoring damage initiation and propagation can be challenging. Non-Destructive Testing (NDT) and Structural Health Monitoring (SHM) techniques can provide valuable insights in the adhesively bonded joints' structural integrity and performance, increasing their reliability and reducing the risks of sudden failure. In particular, Acoustic Emission (AE) has been used in the past to assess damage initiation and propagation by characterising competing damage mechanisms [15–18].

Past research has shown that the stacking sequence strongly affects the composite adhesive joints' damage and failure mechanism [16,19]. The authors reported a strong dependency of the single lap joint strength with the composite bending stiffness. In addition, they demonstrated that certain composite layups could act as a toughening mechanism which deflected the crack from the adhesive (cohesive fracture occurs in the case of small interface ply angles) to the composite (inter/intralaminar fracture occurs for larger interface ply angles). The ply thickness was also shown to strongly affect the performance of composite adhesive joints [20]. The damage initiation and final fracture capacity of adhesive joints were increased significantly with thinner plies, which also led to a more sudden damage progression. More specifically, the damage initiation was increased by 47%, while the failure load was increased by 16% when the ply thickness dropped from 200 μm to 50 μm. Such effects have also been reported based on numerical studies showing that the peak peel and shear stresses were strongly sensitive to the composite ply thickness [21].

The TBDC materials developed by the authors inherently combine different stacking sequences (due to the random tape placement) and very thin plies (as the tape thickness was around 20 μm) [5]. However, the effect of the random orientation of the thin tapes on the adhesive joint performance is currently unclear. The tape ends are expected to lead to multiple stress concentrations over the joint area, resulting in a more uniform stress field in the overlap. The wide range of interface ply angles in Tow-Based Discontinuous Composites (TBDCs) is expected to promote crack deflection from the adhesive layer into the randomly oriented composite tows, potentially giving rise to more complex fracture phenomena - similar to those observed in unidirectional composites with varied stacking sequence angles [16]. Such changes in fracture behaviour may be strategically exploited to enhance the fracture toughness of adhesively bonded joints. Given that a propagating crack tends to follow the path of least resistance, joints bonded with higher-toughness adhesives could benefit from the heterogeneous micro-architecture of TBDCs, triggering crack initiation within the substrate rather than at the adhesive bondline. This study aims to characterise the damage mechanisms in TBDC adhesive joints using a combination of experimental techniques, with a particular focus on evaluating the toughening effects induced by the complex TBDC micro-architecture.

Double Cantilever Beam (DCB) specimens of thin TBDC substrates were manufactured and bonded with a high (> 2400 J/m^2) and a moderate toughness adhesive ($\sim$600 J/m^2). The primary objective was to assess the Mode I fracture toughness of the joints and to investigate the potential toughening mechanisms enabled by the TBDC architecture. The specimens' load-displacement response and crack propagation during testing were monitored. Acoustic Emission (AE) measurements were used to monitor the joint's damage evolution in real time. Fracture surfaces were subsequently examined using both optical and Scanning Electron Microscopy (SEM), and the AE-detected damage events were correlated with observed microstructural features. The focus of the paper was to undertake experimental characterisation of the damage mechanism in adhesively bonded thin TBDCs. To the authors' knowledge, this work presents the first comprehensive investigation of the adhesive bonding behaviour of thin TBDC materials, including a detailed description of their fracture and damage mechanisms. Therefore, the findings of this study open new application potential for this novel material concept, highlighting the significance of the work.

2. Materials and methods

2.1. Experimental testing campaign overview

Four TBDC plates with dimensions 300 × 300 mm and a nominal thickness of 1.2 mm were manufactured. The tapes were produced using the spreading tow technology of TeXtreme using MR70 carbon fibres. The tapes had a nominal width of 20 mm and a nominal length of 40 mm. The TBDC plate manufacturing procedure is described in detail by Katsivalis et al. [5]. The tape and TBDC in-plane properties can be found in Table 1.

The TBDC plates were used to manufacture DCB specimens. The TBDC plates were reinforced with CFRP-UD plies as backup beams to avoid large deformations of the substrates by increasing the specimens' thickness and flexural stiffness. The UD panels were made with HexTow IM7 fibre (fibre modulus 276 GPa), the fibre volume fraction was 60%, and thus the tensile stiffness of the panels was 165 GPa. The thickness of the doublers was 2 mm, which allowed to create a composite DCB arm with significant flexural stiffness (value later calibrated at 140 GPa) which minimised large deformations. Before bonding, the specimens were sanded and degreased and the structural adhesive Hysol 9466 [22] was used for bonding.

Two structural adhesives with distinct fracture toughness characteristics were selected for bonding the DCB arms: Scotch-Weld AF163-2K [23], a high-toughness adhesive with reported Mode I fracture toughness values exceeding 2400 J/m^2 [16]; and Araldite 2015-1 [24], a moderate-toughness adhesive with typical Mode I fracture toughness around 600 J/m^2 [25]. The use of adhesives with contrasting properties was intended to activate different failure mechanisms and thereby broaden the scope of the investigation. For brevity, these adhesives are hereafter referred to as AF and Araldite, respectively. Their material properties are summarised in Table 2. Prior to bonding, the TBDC surfaces underwent surface preparation to ensure optimal adhesion. The surfaces were manually abraded in a criss-cross pattern using 400-grit sandpaper, followed by acetone degreasing. Additionally, a 7-minute ultraviolet (UV) irradiation treatment was applied for surface activation, following the protocol established by the authors in previous work [20].

A thin Teflon tape (thickness of 0.11 mm) was used to introduce an initial delamination zone between the two substrate plates. The bondline thickness for the AF specimens was 0.25 mm, ensured by an embedded nylon carrier. For the Araldite specimens, the bondline thickness was 0.3 mm and was controlled by using three layers of Teflon tape at the initial crack length and a metallic insert at the other edge of the specimen. The TBDC panels were manufactured first (curing temperature 150°C) and were bonded afterwards with the two adhesives at lower curing temperatures (80°C for the Araldite and 120°C for the AF).

Table 1
Tape and in-plane elastic properties for the TBDC plates.

Property	Symbol	Value	Units
Tape longitudinal modulus [a]	E_L	172 ± 5	(GPa)
Tape transverse modulus [a]	E_T	8.11 ± 0.05	(GPa)
Tape Poisson's ratio [a]	ν_{LT}	0.35 ± 0.03	(-)
Tape shear modulus [a]	G_{LT}	2.98	(GPa)
TBDC in-plane modulus [a]	$\overline{E}_x$	70	(GPa)
TBDC in-plane Poisson's ratio [a]	ν	0.33	(-)

[a] Katsivalis et al. [5]

Table 2
Mechanical properties of the adhesives considered.

Property	Scotch-Weld AF163-2k	Araldite 2015-1
Tensile strength (MPa)	46 [b]	23.5 [a]
Maximum elongation at break (%)	5.4 [b]	4.3 [a]
Tensile modulus (MPa)	2043 [b]	1717 [a]
Poisson's ratio	0.34 [c]	0.33 [a]

[a] Saleh et al. [26]
[b] Teixeira de Freitas and Sinke [14]
[c] Scotch-Weld [23]

2.2. DCB testing

The geometry of the DCB specimen can be seen in Fig. 1. The width of the specimens was 25 mm. The cross-section detail shows the composite substrates, consisting of the TBDC and UD material, the adhesive, and the positioning of the Teflon tape. It is worth noting that due to manufacturing limitations the initial pre-crack distance was different for the two adhesives tested. For the Araldite adhesive the distance was 30 mm and for the AF adhesive the distance was 20 mm. A razor blade was used to create a sharp crack while load blocks were used to apply the opening displacements using a 10 kN universal loading machine. The DCB specimens were tested following ASTM standards (ASTM D5528) [27]. A minimum of 4 specimens per adhesive were tested, and the loading rate was adjusted to 1 mm/min.

The complete load-displacement curve was recorded during testing, while the crack front was monitored with a moving optical microscope. Finally, Acoustic Emission (AE) measurements were employed to monitor the damage evolution in the specimens. The Modified Beam Theory (MBT), as shown in Equation (1), was used to determine the fracture toughness for each specimen and to produce the resistance curves (fracture toughness against crack length):

$$G_I = \frac{3P\delta}{2b(a+|\Delta|)} \tag{1}$$

In equation 1, G_I is the mode I fracture toughness, P is the load applied for a given opening displacement δ, while b is the width of the specimen, a is the crack length, and $|\Delta|$ is the portion of the crack length related to the experimental compliance.

2.3. Acoustic Emission (AE) measurements

A Vallen ASMY-6 4-channel acquisition unit (Vallen Systeme GmbH, Icking, Germany) was connected to a 34 dB AEP5 preamplifier linked with Vallen VS900-M broad frequency piezoelectric transducer sensors (resonant working frequency between 100-900 kHz). The sensor used on the specimens had a diameter of 20.3 mm and a height of 14.3 mm with a total weight of 22 g. It is worth mentioning that a single sensor was used for the DCB testing, and it was clamped to the specimens using a manual pressure clamping tool to maintain it in position during the experimental tests and prevent any additional vibration caused by the sensor's movement.

Magnaflux ultra gel II was used to couple the sensor in the specimen's surface to ensure the continuous transmission of AE signals from the material to the sensors. Before the experimental tests, pencil lead break testing (Hsu-Nielsen [28]) was performed to determine the acquisition parameters, make adjustments to reduce the background noise during testing and check the sensor's functionality. The Vallen AE-suite R2019.0926.1 software was used for data logging. The AE data acquisition was synchronised with the load and displacement from the testing machine, allowing their direct correlation with the experimental data. Table 3 summarises the AE acquisition parameters.

2.4. AE post-processing

Acoustic Emission (AE) data were continuously recorded throughout the DCB tests and captured in two primary raw data formats: (a) time-domain features, including maximum amplitude, rise time, duration, energy, threshold (user-defined), counts (the number of times the AE waveform crosses the threshold), and decay time; and (b) waveform transients, consisting of amplitude and sampling time. Frequency-domain features, such as peak and centroid frequency, were subsequently derived from the transient waveforms. To improve signal fidelity and eliminate background noise, a filtering procedure was applied to the dataset. All AE signals with count values less than or equal to two were excluded from further analysis. This filtering step removed, on average, approximately 20% of the total recorded waveforms.

Following data cleaning, the remaining AE signals were clustered using unsupervised machine learning techniques - specifically Self-Organising Maps (SOM) and k-means clustering. These algorithms were implemented using a custom MATLAB script developed by the authors, as described in detail in [29]. The clustering methodology is illustrated in the workflow shown in Fig. 2. Accurate clustering and classification of AE waveforms based on their intrinsic characteristics and correlation with experimental load–displacement data is critical for interpreting both visible and sub-surface damage mechanisms. This approach enables a comprehensive understanding of the failure processes occurring in the TBDC adhesive joints during Mode I fracture.

As shown in Fig. 2, the acoustic emission time and frequency domain features were first extracted. After filtering, the clustering methodology selected the most relevant features for separating the AE waveforms, considering the maximisation of the data variance. The energy and peak frequency values for each remaining AE waveform were used as the main input values for the SOM algorithm, in which a 2D topological map

Table 3
AE acquisition parameters.

Parameters	Values
Sampling rate for the acquisition of the AE features	10 MHz
Sampling rate for the AE waveforms acquisition	2 MHz
Digital pass-band frequency filter for the AE waveforms	25-850 kHz
Amplitude – threshold	34 dB
Rearm Time	400 μs
Duration discrimination time (time window to register each AE signal)	400 μs

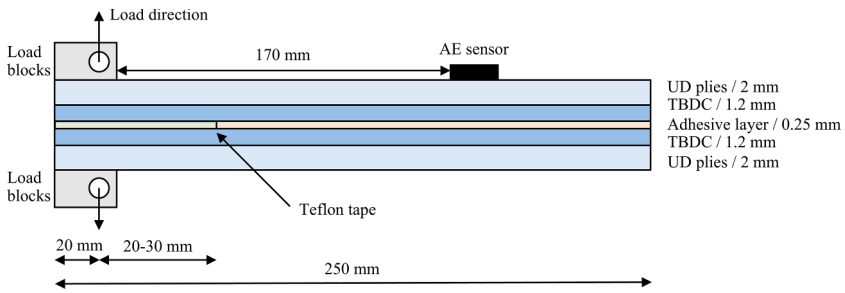

Fig. 1. Sketch of the cross-section of the DCB specimen (dimensions not to scale).

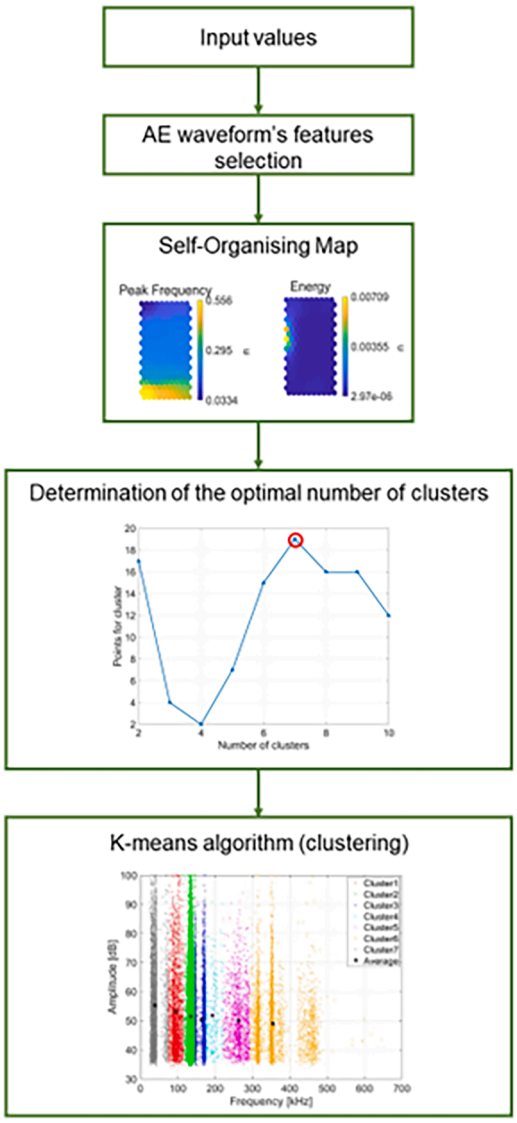

Fig. 2. Workflow of the AE clustering methodology.

was created, positioning the data with similar characteristics closer together considering their Euclidean distance. The SOM algorithm was not sufficient in dividing the data into a specific number of groups and thus an optimal number of clusters was defined based on indexing scoring, as explained in [15,29]. An optimal number of seven clusters was determined. Finally, the k-means algorithm was applied, dividing the whole dataset into the defined optimal number of clusters which changed depending on the specimen type.

2.5. Post-failure microscopy analysis

After the mechanical testing of the specimens, post-mortem fracture analysis was performed on a macroscopic and microscopic level. The Keyence VR5000 Wide-area 3D profiling system was used for the former to take high-quality images of the complete failure surfaces and identify the macroscopic damage mechanisms. This analysis allowed the identification of the crack propagation during testing and the damage transition areas (from substrate to adhesive/cohesive damage).

Scanning Electron Microscopy (SEM) was used for the microscopic analysis to evaluate the interfaces of the tested specimens. Representative areas of the specimens were selected for the SEM analysis. A thin layer of gold sputter (about 5 μm) was applied to the specimens to reduce the electric charging and attain high-quality images. Afterwards, the specimens were mounted on stubs and analysed with a JEOL 7800F Prime. The microscope magnifications were between x100 and x5000, and the acceleration voltage ranged between 2 and 10 kV.

3. Results

3.1. Mechanical testing

Fig. 3 shows the load/displacement curves obtained for the DCB specimens bonded with the AF and Araldite adhesives. The grey shaded area corresponds to the experimental scatter of the AF specimens while the red shaded area corresponds to the experimental scatter of the Araldite specimens. The response of the AF specimens in the initial, linear part of the load/displacement curve is significantly stiffer, which can be explained by the different initial crack lengths between the two types of specimens. More specifically, the length of the initial delamination was 30 mm for the Araldite specimens but only 20 mm for the AF specimens due to manufacturing limitations. Fig. 3 also shows that the AF specimens reached a higher load peak before the softening region. After the peak load, a higher scatter was also observed for both adhesives. The thin TBDCs inherently have higher scatter when compared to typical laminates due to the random tape orientation. Such observations were made in independent TBDC tests under tension [5], compression [6] and fatigue [7] loading. This effect is exacerbated in the DCB specimens as the damage is controlled by the DCB interfaces and thus the relative tape orientation becomes even more significant. The higher scattering in the load versus displacement curve can also be associated with the migration of cracks through the tapes as the crack progresses, which may result in multiple delamination fronts in the composite, as seen later in Fig. 5.

Fig. 4 shows characteristic fracture surfaces of the DCB specimens for the Araldite and AF adhesives. All specimens displayed a certain degree of scattering, which can be justified by the different damage mechanisms developed during damage propagation. More specifically, the Araldite DCB specimens displayed a combination of substrate and adhesive/cohesive failure in various parts of the specimens (Fig. 4a). In contrast, the only damage mechanism observed in the AF specimens was the delamination of the TBDC tapes (Fig. 4b).

Fig. 5 shows the Araldite and AF specimens' R-curves (fracture toughness/crack length). The crack deflected from the TBDC/adhesive interface for two Araldite specimens and moved to the reinforcement/TBDC interface, where it propagated. Therefore, the data points after the crack deflection were omitted from the figure. The horizontal line in Fig. 5a indicates a value of 600 J/m^{2,} typically cited as the mode I

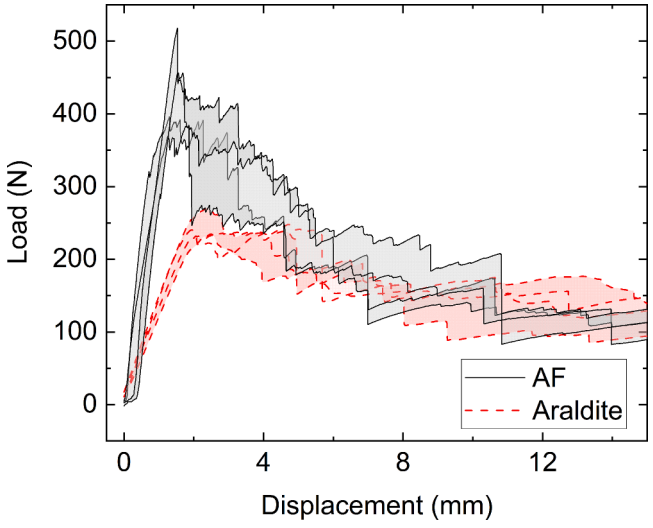

Fig. 3. Load-displacement curves for the AF and Araldite DCB specimens.

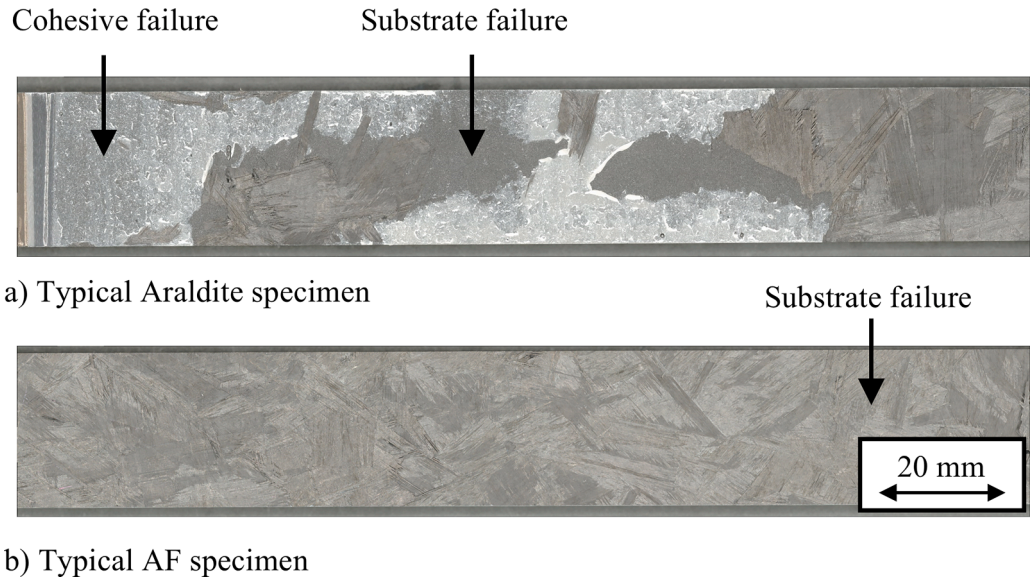

Fig. 4. Typical fracture surfaces of the DCB specimens for the a) Araldite and b) AF specimens.

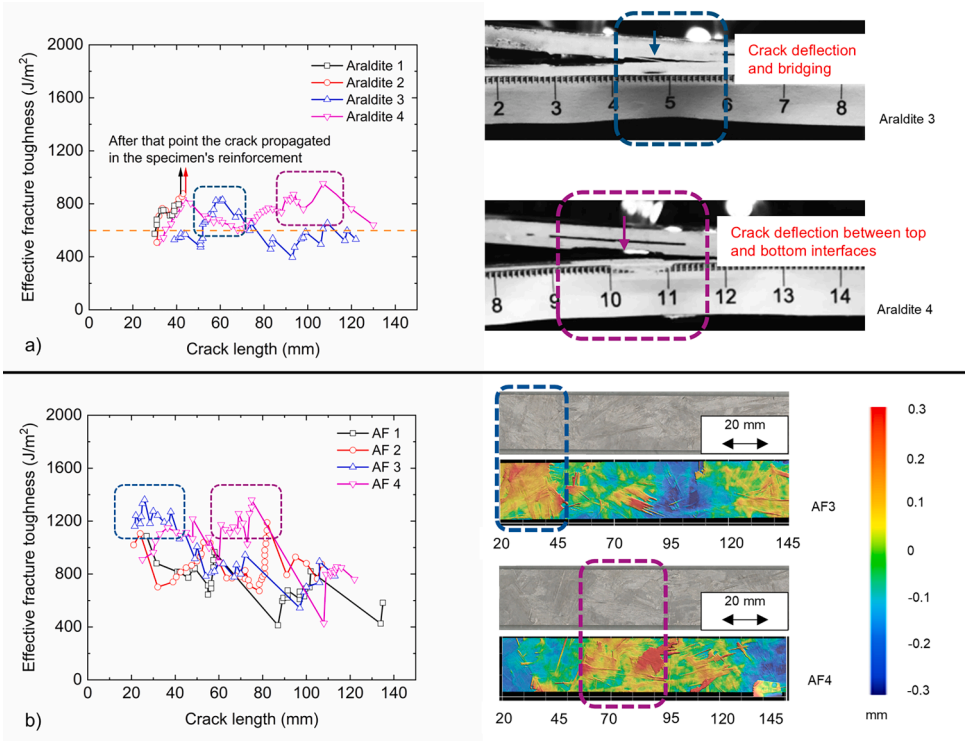

Fig. 5. Analysis of the effective fracture toughness for the a) Araldite and b) AF specimens. For the Araldite specimens, additional side views are provided which highlight the crack deflection. For the AF specimens, additional fracture surfaces are provided which highlight the fracture surface topology.

fracture toughness of the Araldite adhesive under cohesive failure [16]. Most of the data points are above this value, indicating a toughening effect that the TBDC architecture has on the performance of the DCB specimens.

In addition, Fig. 5a focuses on two areas of elevated values of fracture toughness for specimens Araldite 3 and Araldite 4 and displays the recordings of the cameras used for crack monitoring. In Araldite 3, there is a fracture toughness peak around crack length of 50-60 mm. The side views reveal crack deflection from the bottom to the top interface and tape bridging. A similar area of increased fracture toughness was spotted for Araldite 4 at crack length of about 90-120 mm and the side view of the specimen revealed crack deflections between the bottom and top interfaces.

For the AF specimens, the damage initiation occurred in the composite material and did not migrate to the adhesive or the specimen's reinforcement. The crack only propagated inside the composite, and the random orientation of the tapes controlled the propagation mechanism. The fact that the damage propagated exclusively in the composite highlights that the AF adhesive has significantly higher fracture toughness than the TBDC composite. The tape stacking and orientation created smaller interfaces with random angle differences, which can explain the large scatter in the fracture toughness measurements

(ranging from 400 to 1400 J/m^2).

Further analysis of the fracture surfaces for the AF specimens, revealed elevated fracture toughness values for AF3 (crack length 25-40 mm) and AF4 (crack length about 60-80 mm). As shown in Fig. 5b, these fracture toughness peaks correspond to higher values of surface topography (around 0.3 mm). In Fig. 5b, lower values of surface topography correspond to the areas closer to the interface while higher values correspond to areas further away from the interface. As the crack travels deeper into the TBDC, the fracture field possibly expands, with more space for multiple crack deflection, crack branching and possible tape bridging. These complex fracture phenomena lead to reduction of the energy input in the main crack tip and therefore an increase in the measured energy fracture resistance. On the contrary, when the crack travels within the TBDC but close to the interface with the adhesive layer, the fracture space is constrained leaving less room for the toughening mechanisms of the TBDC to develop. This highlights the potential of using thin TBDCs as toughening layers in composite bonded structures and will be further explored in section 4.2. Table 4 summarises the fracture toughness measurements for the two adhesives.

It is worth noting that due to the damage propagating in the composite (and not in the midplane of the bondline) some minor mode-mixity was introduced in the specimens which justifies the use of the term effective fracture toughness in the y axis of Fig. 5. This is a common strategy when analysing thicker joints [25]. In such cases, the cracks can deviate from the midplane, but it is still valid to extract the value for the effective toughness of the joint.

In summary it was possible to observe that:

- The Araldite adhesive has fracture toughness which is within the identified toughness of the TBDC substrates. Therefore, the random distribution of the tows had an impact in the crack propagation path, created stress concentrations which triggered crack deflections throughout the TBDC or cohesive crack propagation. These two competing mechanisms created potential for the crack to deflect between the adhesive and the TBDC, resulting in a toughening effect.
- The AF adhesive has fracture toughness significantly higher compared to the TBDC substrate and thus the crack path migrated directly to the TBDC at crack onset and remained there. The higher variation in the fracture toughness of the AF specimens was related to the location of the crack. As the crack moved away from the interface, multiple crack fronts were generated between the tapes, leading to toughening effects.

3.2. AE damage characterisation results

The acoustic emission clustering analysis (presented in Fig. 2) was performed for each DCB specimen. The acoustic emission signals' energy and calculated peak frequencies were input values for the SOM topographic map creation. It was found that the dataset's optimal number of clusters was 7. Fig. 6 shows the filtered acoustic emission data (around 60,000 waveforms for each specimen) before and after clustering for the Araldite and the AF DCB specimens.

Fig.s 6a and 6b show that the main acoustic emission activity starts after the first load peak is reached. After that, a clustering method based on combining the SOM and K-means algorithm was performed using the energy and peak frequency values as the main input features. An optimal number of clusters was defined based on the scoring performance of the most used indexing criteria found in the literature (i.e., Calinski-Harabasz, Davies-Bouldin, and Silhouette), as described in [30].

The peak frequency values significantly influenced the division of the acoustic emission data sets, leading to seven main groups for the DCB specimens (Fig.s 6c and 6d). Frequency is commonly used for clustering and classifying the acoustic emission datasets acquired from composite material testing [31]. Acoustic emission waveforms with low-frequency values often correlate with matrix cracking, while high-frequency values mostly correlate with fibre breakage [31]. It is challenging, however, to identify corresponding damage mechanisms for the intermediate frequency values.

Recent work by the authors investigated how clustered acoustic emission data can aid the understanding of the damage mechanisms of tailored composite adhesively bonded joints under mode I loading conditions [15]. This previous work determined six main clusters according to their energetic properties and time-frequency spectrograms. In addition, a damage mechanism was linked to each of these clusters as shown in Table 5.

It can be observed that the majority of the clusters identified from the DCB TBDC specimens (Fig. 6c and 6d) exhibit comparable average frequency values as those reported in [15]. In addition, the substrates of our study demonstrate comparable mechanical properties to those studied in [15]. Therefore, it can be assumed that they represent the same damage mechanisms. Two new clusters were identified in the current study only for the DCB specimens: clusters (b) and (c) at 87 kHz and 100 kHz peak frequency, respectively. Furthermore, cluster (h), with a peak frequency of 147 kHz, was only defined at the Araldite DCB specimens.

It is important to highlight that, as seen in Fig.s 6c and 6d, for the specimens bonded with the AF adhesive, the clustering algorithm grouped a range of AE signals that vary from 130 to 147 kHz average peak frequency. For the specimens bonded with the Araldite adhesive, waveforms in this frequency range were divided into two groups instead.

The recently identified clusters, at 87 kHz, 100 kHz, and 147 kHz, are likely associated with the damage mechanisms caused by void nucleation and coalescence of the adhesive layer. However, further investigation would be necessary to confirm this association due to the complicated nature of the damage evolution in these specimens and the damage related to the backup beam of the DCB specimens. Characterising the most relevant damage mechanisms for the failure of the proposed adhesively bonded joints is crucial in loading conditions where sudden failure is observed. In particular, the acoustic emission monitoring system can give relevant insights into damage accumulation within the joint.

Table 4
Summary of fracture toughness measurements for the two adhesives highting the maximum and minimum values recorded for each specimen.

Specimen	Maximum fracture toughness (J/m2)	Minimum fracture toughness (J/m2)
Araldite 1	795	573
Araldite 2	875	508
Araldite 3	824	396
Araldite 4	876	514
Average	*842 ± 35*	*498 ± 64*
AF 1	1085	412
AF2	1189	701
AF3	1333	543
AF4	1360	428
Average	*1241 ± 111*	*521 ± 115*

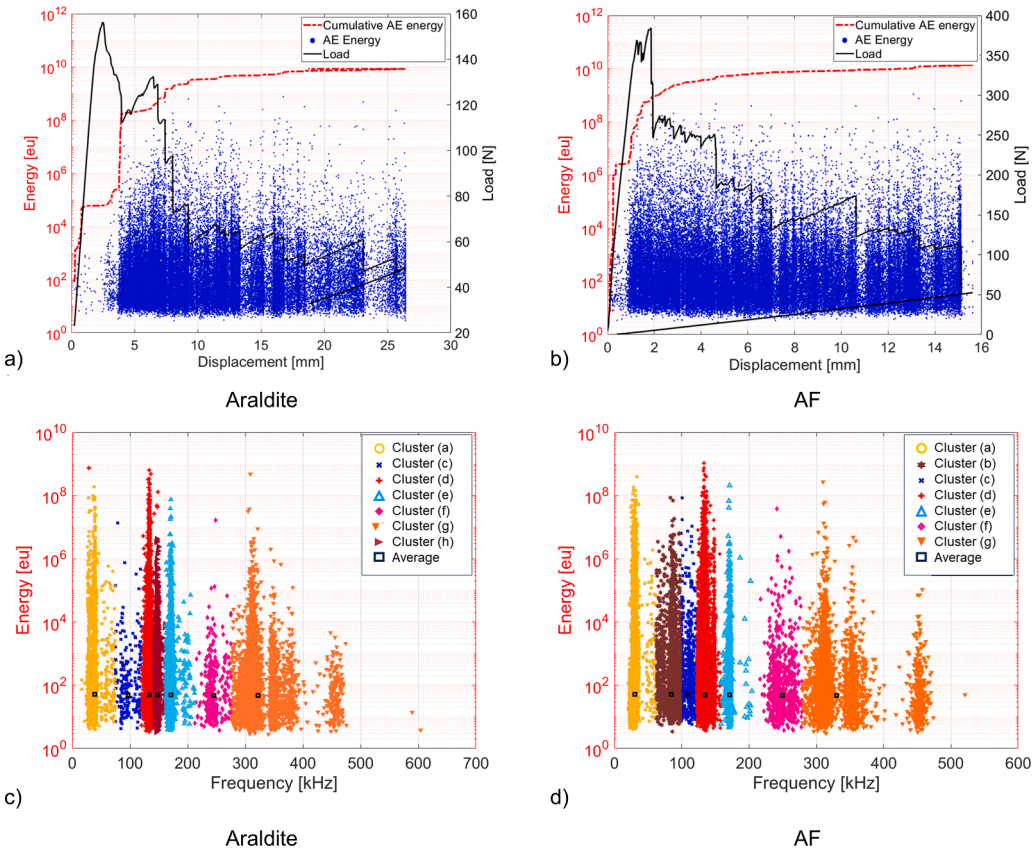

Fig. 6. Acoustic emission data after filtering (a and b) and after clustering (c and d) using energy and peak energy for both adhesives: Araldite (a) and (c); AF (b) and (d).

Table 5
Summary of the peak frequencies identified in [15] and correspondent damage mechanisms.

Peak Frequency per cluster as identified in [15] (kHz)	Assigned damage mechanism
35	Micro-cracking
60	Delamination
130	Matrix cracking
170	Fibre-matrix debonding
255	Fibre pull-out
>300	Fibre breakage

4. Discussion

4.1. Fractographic analysis

The analysis of the fracture surfaces described in Sections 3.1 and 3.2 focused on identifying macroscopic damage features, such as composite damage and adhesive or cohesive damage. However, insights gained from the acoustic emission data indicate the presence of multiple coexisting damage mechanisms in adhesively bonded TBDC materials, which underscores the need for further investigation. As noted by Saeedifar and Zarouchas [31] using peak frequencies of waveforms as a primary feature for clustering acoustic emission data in composite materials is a common approach. The established correlations between matrix cracking and fibre breakage, associated with low and high peak frequency values, are well-documented in the literature.

It is important to recognize that variations in the frequency ranges attributed to the same damage mechanisms can occur across different studies [15,16,31]. These variations depend on factors such as material types, loading conditions, and environmental influences. This inconsistency indicates that while identifying damage mechanisms is valuable, we are still far from establishing a definitive correlation between peak frequency values and most damage mechanisms in adhesively bonded composite materials. To gain a deeper understanding, further analysis of the fracture surfaces was conducted using scanning electron microscopy (SEM). Multiple specimens and fracture surfaces were examined for each test, and Fig.s 7 and 8 present characteristic examples that highlight features observed consistently.

Different magnifications were used to identify the more/less microscopic damage features. For the Araldite specimens, the analysis focused on the areas of damage transition from the composite to the adhesive, as shown in Fig. 7. Fig. 7a shows the exact location of the damage transition at a magnification of x100. Fig.s 7b and 7c show these locations in higher magnification levels (x500).

Fig. 7b shows the cohesive damage within the adhesive layer which developed due to growth and coalescence of voids as demonstrated by the unstructured resin deformation. The most dominant damage mechanism on the composite side is fibre breakage, while limited matrix deformation can also be observed. The AE readings identified the fibre breakage through cluster (g), while the cohesive damage and the matrix deformation were identified through clusters (d) and (h) – see Fig. 6c.

SEM analysis was also performed on the AF specimens shown in Fig. 8. The analysis revealed extensive fibre breakage throughout the specimen. There was also evidence of matrix deformation, but this was less extended. Finally, matrix nano-porosity was also observed as residue in the fibres (Fig. 8c). These observations validate the clustering methodology of the AE analysis as the micro (cluster (a)) and macro matrix cracking (cluster (d)), the fibre/matrix debonding (cluster (e)) and the fibre breakage clusters (cluster (g)) were well represented in the AE data. It is worth noting that the nano-porosity is related to this specific reactive binder matrix and was observed by the authors in previous publications involving the same material system [5].

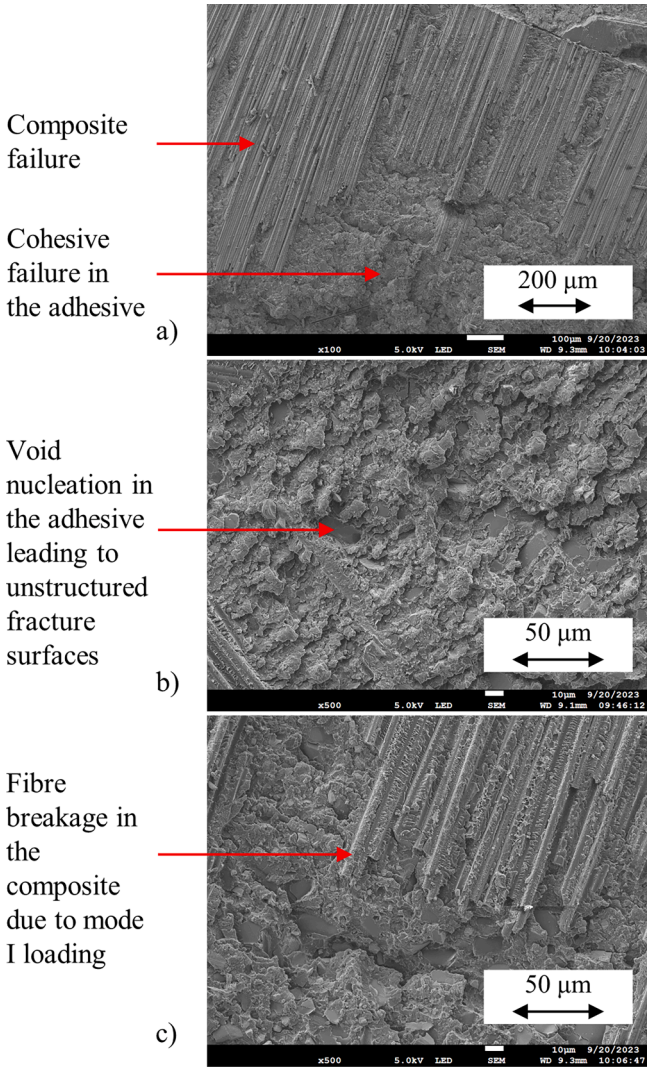

Fig. 7. SEM imaging for a characteristic Araldite DCB specimen across different scales showing a) the combined composite and adhesive failure, b) the cohesive damage in the adhesive layer, c) the fibre breakage in the composite.

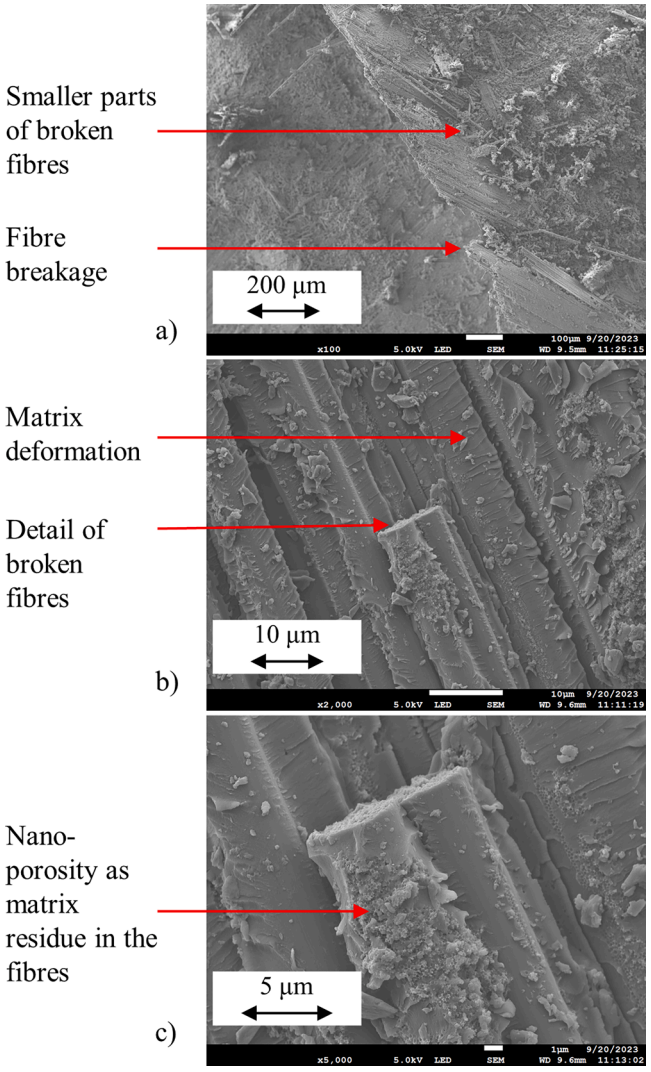

Fig. 8. SEM imaging for a characteristic AF DCB specimen across different scales showing a) the substrate failure, b) details of the broken fibres, c) the nano-porosity found in the matrix residue found in the fibres.

The main findings from the Acoustic Emission (AE) analysis are consistent with the authors' previous work [15] and have been further validated by post-mortem fractographic examination using Scanning Electron Microscopy (SEM). Specifically, SEM analysis confirmed that matrix cracking and fibre/matrix debonding were the predominant damage mechanisms - correlating well with AE data, particularly clusters (d) and (e), which exhibited dominant peak frequencies at approximately 130 kHz and 170 kHz, respectively (see Fig.s 6c, 6d).

It is noteworthy that only a limited number of studies have applied AE techniques to investigate damage evolution in adhesively bonded joints. In the present study, matrix-related damage mechanisms were generally associated with lower-frequency AE signals, while fibre-dominated failures corresponded to higher peak frequencies. These observations are in line with trends reported in existing literature [15, 17–19,30,31]. The matrix-related damage can occur within the adhesive layer in the bonded joints (cohesive failure), but it can also be correlated with the matrix-cracking in the composite laminates. It is likely that the mechanical and acoustic characteristics of the adhesive and substrate polymers are too similar, making it difficult for AE clustering alone to reliably separate these two failure modes.

Nonetheless, the variability in frequency ranges reported for cohesive and adhesive failures across different studies underscores the need for a critical approach in AE data post-processing. Specifically, the selection of clustering parameters - including the number of clusters and input features - should not rely solely on fixed rules or literature assumptions. Instead, these decisions must be tailored to the material system, joint configuration, and loading conditions under investigation to ensure meaningful interpretation.

Despite the challenges in refining AE clustering methodologies, this study reinforces the technique's potential for identifying early-stage damage and distinguishing between failure modes. When combined with advanced imaging and data-driven tools, AE analysis offers a powerful framework for evaluating damage progression and can significantly contribute to the design and structural health monitoring of complex composite systems such as TBDCs.

5. Conclusions

Thin TBDCs are expected to play a significant role in the design of aerospace and automotive structures in the future. However, currently, there is a complete lack of studies on the bonding methods of TBDCs. The damage mechanisms of TBDC adhesively bonded joints under mode I loading using DCB testing are analysed using a range of experimental and monitoring techniques, including macroscopic analysis of the global joint response, damage characterisation using AE, and microscopic and fractographic analysis. Based on the results and discussion, the following

conclusions can be drawn:

- The DCB testing revealed that for the moderate toughness adhesive (around 600 J/m^2), the damage was mostly restricted in the bondline and did not migrate to the TBDC composite. This aligns with previous observations by the authors for UD and cross-ply laminates.
- For the DCB specimens bonded with the high toughness adhesive (> 2400 J/m^2), the damage initiated and propagated in the composite TBDC micro-architecture. The authors also made similar observations for conventional cross-ply and multi-directional laminates bonded with the same adhesive. The mode I fracture toughness values recorded were in the region of 800 J/m^2 (with large experimental scatter). This is significantly higher compared to typical values for damage propagating in UD (around 300 J/m^2) and cross-ply laminates and highlights the potential of using thin TBDCs as toughening layers in composite bonded structures.
- Detailed analysis of the AE activity showed that the damage profile of the DCB specimens was complex and many competing damage mechanisms co-existed. The most pronounced damage mechanisms were matrix cracking and fibre/matrix debonding. The post-mortem fractography analysis in SEM validated these findings.
- The insights gained here provide ideas for future work in exploring the concept of utilising thin TBDCs as toughening layers in continuous CFRP laminates. In addition, pure mode II testing of TBDC adhesive joints can also be performed, which could possibly expand the design space of these material even further.

In summary, this paper provides first study relating to the adhesive bonding of TBDCs and demonstrates the importance of adhesive toughness on the damage mechanism and fracture toughness, with implication for aerospace and automotive applications.

CRediT authorship contribution statement

Ioannis Katsivalis: Writing – original draft, Software, Methodology, Investigation, Funding acquisition, Formal analysis, Data curation, Conceptualization. **Rosemere de Araujo Alves Lima:** Writing – original draft, Software, Methodology, Investigation, Formal analysis, Data curation, Conceptualization. **Florence Moreau:** Writing – review & editing, Resources. **Leif E. Asp:** Writing – review & editing, Methodology, Investigation, Funding acquisition, Formal analysis, Conceptualization. **Sofia Teixeira de Freitas:** Writing – review & editing, Methodology, Investigation, Funding acquisition, Formal analysis, Conceptualization.

Declaration of competing interest

The authors declare that they have no known competing financial interests or personal relationships that could have appeared to influence the work reported in this paper.

Acknowledgments

The authors would like to acknowledge funding from the Swedish Energy Agency via its Competence Centre Technologies and innovations for a future sustainable hydrogen economy (TechForH2, dnr. 2021-036176). The authors would also like to acknowledge the support of the COST (European Cooperation in Science and Technology) Action CA18120 (CertBond). The authors acknowledge Fundação para a Ciência e a Tecnologia (FCT) for its financial support via the project LAETA Base Funding (DOI: 10.54499/UIDB/50022/2020).

Data availability

Data will be made available on request.

References

[1] Y. Li, S. Pimenta, J. Singgih, S. Nothdurfter, K. Schuffenhauer, Experimental investigation of randomly-oriented tow-based discontinuous composites and their equivalent laminates, Compos. A: Appl. Sci. Manuf. 102 (2017) 64–75.
[2] S.G. Kravchenko, D.E. Sommer, B.R. Denos, A.J. Favaloro, C.M. Tow, W.B. Avery, R.B. Pipes, Tensile properties of a stochastic prepreg platelet molded composite, Compos. A: Appl. Sci. Manuf. (2019) 124.
[3] S.G. Kravchenko, D.E. Sommer, R.B. Pipes, Uniaxial strength of a composite array of overlaid and aligned prepreg platelets, Compos. A: Appl. Sci. Manuf. 109 (2018) 31–47.
[4] M. Alves, D. Carlstedt, F. Ohlsson, L.E. Asp, S. Pimenta, Ultra-strong and stiff randomly-oriented discontinuous composites: Closing the gap to quasi-isotropic continuous-fibre laminates, Compos. A: Appl. Sci. Manuf. 132 (2020) 105826.
[5] I. Katsivalis, M. Persson, M. Johansen, F. Moreau, E. Kullgren, M. Norrby, D. Zenkert, S. Pimenta, L.E. Asp, Strength analysis and failure prediction of thin tow-based discontinuous composites, Compos. Sci. Technol. 245 (2024) 110342.
[6] I. Katsivalis, A. Tongloet, X. Wu, M. Norrby, F. Moreau, S. Pimenta, M.R. Wisnom, D. Zenkert, L.E. Asp, Compressive properties of thin tow-based discontinuous composites, Compos. B: Eng. 292 (2025) 112085.
[7] I. Katsivalis, M. Norrby, F. Moreau, E. Kullgren, S. Pimenta, D. Zenkert, L.E. Asp, Fatigue performance and damage characterisation of ultra-thin tow-based discontinuous tape composites, Compos. B: Eng. 281 (2024) 111553.
[8] P.P. Camanho, C.G. Dávila, S.T. Pinho, L. Iannucci, P. Robinson, Prediction of in situ strengths and matrix cracking in composites under transverse tension and in-plane shear, Compos. A: Appl. Sci. Manuf. 37 (2006) 165–176.
[9] J. Galos, Thin-ply composite laminates: a review, Compos. Struct. 236 (2020) 111920.
[10] L.M. Martulli, L. Muyshondt, M. Kerschbaum, S. Pimenta, S.V. Lomov, Y. Swolfs, Carbon fibre sheet moulding compounds with high in-mould flow: Linking morphology to tensile and compressive properties, Compos. A: Appl. Sci. Manuf. 126 (2019) 105600.
[11] M. Selezneva, L. Lessard, Characterization of mechanical properties of randomly oriented strand thermoplastic composites, J. Compos. Mater. 50 (2015) 2833–2851.
[12] L.F.M. da Silva, A. Öchsner, R.D. Adams, Handb. Adhes. Technol.: Second Ed. (2018).
[13] L. da Silva F M, R. D Adams, Techniques to reduce the peel stresses in adhesive joints with composites, Int. J. Adhes. Adhes. 27 (2007) 227–235.
[14] S. Teixeira de Freitas, J. Sinke, Failure analysis of adhesively-bonded skin-to-stiffener joints: Metal–metal vs. composite–metal, Eng. Fail. Anal. 56 (2015) 2–13.
[15] R.A.A. Lima, R. Tao, A. Bernasconi, M. Carboni, S. Teixeira de Freitas, Acoustic emission approach for identifying fracture mechanisms in composite bonded Joints: A study on varying Substrate's stacking sequence, Theor. Appl. Fract. Mech. 132 (2024) 104490.
[16] R.A.A. Lima, R. Tao, A. Bernasconi, M. Carboni, N. Carrere, S. Teixeira de Freitas, Uncovering the toughening mechanisms of bonded joints through tailored CFRP layup, Compos. B: Eng. 263 (2023) 110853.
[17] C. Yildirim, H. Ulus, B. Beylergil, A. Al-Nadhari, S. Topal, M. Yildiz, Tailoring adherend surfaces for enhanced bonding in CF/PEKK composites: Comparative analysis of atmospheric plasma activation and conventional treatments, Compos. A: Appl. Sci. Manuf. 180 (2024) 108101.
[18] C. Yildirim, H. Ulus, H.S. Sas, S. Topal, M. Yildiz, Assessing the fracture and dynamic mechanical performance of CF/PEKK joints bonded with epoxy-based adhesive film for aerospace applications: Impact of thermal and cycling hygrothermal conditions, Compos. A: Appl. Sci. Manuf. 190 (2025) 108659.
[19] J. Kupski, S. Teixeira de Freitas, D. Zarouchas, P.P. Camanho, R. Benedictus, Composite layup effect on the failure mechanism of single lap bonded joints, Compos. Struct. 217 (2019) 14–26.
[20] J. Kupski, D. Zarouchas, S. Teixeira de Freitas, Thin-plies in adhesively bonded carbon fiber reinforced polymers, Compos. B: Eng. 184 (2020) 107627.
[21] H. Bendemra, P. Compston, P.J. Crothers, Optimisation study of tapered scarf and stepped-lap joints in composite repair patches, Compos. Struct. 130 (2015) 1–8.
[22] Loctite, LOCTITE EA 9466 - Technical Data Sheet, 2014.
[23] Scotch-Weld, 3M Scotch-Weld AF 163-2K, 2009.
[24] Huntsman, Araldite 2015-1 Technical Datasheet, 2016. Basel.
[25] R. Lopes Fernandes, S. Teixeira de Freitas, M.K. Budzik, J.A. Poulis, R. Benedictus, From thin to extra-thick adhesive layer thicknesses: Fracture of bonded joints under mode I loading conditions, Eng. Fract. Mech. 218 (2019) 106607.
[26] M.N. Saleh, M.K. Budzik, M. Saeedifar, D. Zarouchas, S. Teixeira De Freitas, On the influence of the adhesive and the adherend ductility on mode I fracture characterization of thick adhesively-bonded joints, Int. J. Adhes. Adhes. 115 (2022) 103123.

[27] ASTM, ASTM D5528/D5528M-21, Standard Test Method for Mode I Interlaminar Fracture Toughness of Unidirectional Fiber-Reinforced Polymer Matrix Composites, ASTM International, West Conshohocken, PA, 2022, p. 2022.
[28] K. Ono, Calibration Methods of Acoustic Emission Sensors, Materials (2016).
[29] R.A.A. Lima, M. Drobiazko, A. Bernasconi, M. Carboni, On crack tip localisation in quasi-statically loaded, adhesively bonded double cantilever beam specimens by acoustic emission, Theor. Appl. Fract. Mech. 118 (2022) 103286.
[30] D. Crivelli, M. Guagliano, A. Monici, Development of an artificial neural network processing technique for the analysis of damage evolution in pultruded composites with acoustic emission, Compos. B: Eng. 56 (2014) 948–959.
[31] M. Saeedifar, D. Zarouchas, Damage characterization of laminated composites using acoustic emission: A review, Compos. B: Eng. 195 (2020) 108039.